Many-body dispersion forces of polarizable clusters and liquids

J. Cao[a] and B. J. Berne
Department of Chemistry and Center for Biomolecular Simulations, Columbia University, New York, New York 10027-6948

(Received 10 July 1992; accepted 24 August 1992)

A system of atoms with embedded Drude dispersion oscillators interacting through dipole–dipole forces is simulated. Using path integrals it is shown that after the coordinates of the dispersion oscillators are integrated out, the atoms interact through many-body dispersion forces to all orders of the dipole–dipole interaction. Simulations are carried out on clusters to see if the presence of many-body forces leads to ground state geometries different from those predicted from two-body potentials. In addition, the polarizability tensor of clusters is determined as a function of cluster size. Simulations are also carried out for fluids to see how many-body forces affect the pair correlation function. Lastly, the long-range interaction between van der Waals clusters is compared with the predictions of a summation over site–site two-body interactions. It is found that many-body forces have only a minor effect on the low energy geometries of van der Waals clusters, a somewhat surprising result given that many-body forces do give an important contribution to surface free energies of clusters and liquids. The vibrational frequencies of the breathing mode decrease by approximately 10%.

I. INTRODUCTION

The structure and dynamics of condensed systems is determined by the total intermolecular interaction potential. In theoretical and numerical studies the total potential is often approximated as a superposition of pair potentials consisting of a short-range repulsive part (r^{-12}) arising from overlap and exchange interactions and a long-range attractive part (r^{-6}) arising from correlated dipole–induced-dipole interactions. Although this approximation often suffices for the determination of the thermodynamic properties of simple dense fluids, it fails to adequately account for gas phase properties[1] and for surface properties of liquids.[2] It is now well known that the surface tension predicted by a pairwise additive potential of the Lennard-Jones (12–6) [L-J (12–6)] form gives surface tensions in error by as much as 50%. In this case the use of the Axilrod–Teller three-body potential corrects the surface tension.[1]

Hoare and Pal[3] have determined the geometries of van der Waals clusters as a function of cluster size for atoms interacting through the L-J (12–6) potential. These are the so-called minimum energy geometries. Because surface properties are sensitive to many-body forces one wonders if these geometries will be the same if many-body forces are included.

In this paper we incorporate many-body forces in a simple way by implanting in each atom a three dimensional isotropic Drude dispersion oscillator of mass m, charge q, frequency ω, and polarizability $\alpha=q^2/m\omega^2$. Although these dispersion oscillators interact through Coulomb's law, we consider a simplified model in which they interact through dipole–dipole forces. This model has been widely used to calculate the dielectric properties and absorption spectra of nonpolar polarizable fluids and clusters.[4–7] Path integral methods allow us to formulate this many-body problem as a matrix problem when the dipole–dipole approximation is used. We are able to transform the dipole–dipole interaction to normal modes and thus find the interaction energy in a simple, computationally efficient way. Solution of the resulting matrix problem allows us to determine the lowest energy geometries of van der Waals clusters including three-body, four-body, ..., N-body interactions as well as many-body effects on the structure of bulk liquids. The same analysis allows us to determine the many-body contribution to the polarizability tensor of clusters.

We find that the lowest energy geometries of van der Waals clusters with many-body forces are essentially the same as those for clusters with two-body interactions as given by Hoare and Pal,[3] but that these clusters are expanded by up to 3% in volume. Furthermore we find that the vibrational frequencies of the clusters are smaller by 10%. This insensitivity of structure to the presence of many-body forces is surprising given that in liquids they lead to a dramatic reduction in the surface free energy of the gas–liquid interface. We also find that many-body forces perturb the radial distribution function of liquids by slightly decreasing the size of the first peak and leads to an increase in the attractive interaction between clusters at large separations over what would be predicted by the superposition of site–site two-body forces.

There have been several papers on the many-body interactions in clusters.[8–12] The three-body correction for the helium trimer has been the topic of considerable interest.[12,13] Given that the polarizability of helium is small, it is not likely that a dispersion oscillator model will be a good approximation to it. The dominant contribution to the interaction in helium is the exchange potential, a topic not

[a]In partial fulfillment of the Ph.D. in the Department of Physics, Columbia University.

 0021-9606/92/238628-09$006.00

treated in this paper. Recently, it was found that three-body forces give important corrections to the vibrational spectrum of Ar_3.[10] Also, many-body polarization is a critical factor in constructing nonpairwise interaction potentials of large clusters from information about small clusters.[9,14] This paper presents a systematic study of the dipolar polarization effects on clusters ranging from 7 to 26 rare gas atoms.

II. THE DISPERSION OSCILLATOR MODEL

The Hamiltonian for a Drude oscillator of charge q, mass m, frequency ω, and polarizability $\alpha=q^2/m\omega^2$, i.e., a dispersion oscillator, with instantaneous dipole $\mathbf{p}_i$ is[7,15]

$$H_0(\mathbf{p}_i,\dot{\mathbf{p}}_i)=\frac{\dot{\mathbf{p}}_i^2}{2\alpha\omega^2}+\frac{\dot{\mathbf{p}}_i^2}{2\alpha}. \tag{2.1}$$

The Hamiltonian for a fluid composed of N harmonious atoms (atoms with implanted Drude oscillators) coupled through their instantaneous dipole moments is then

$$H=\sum_{j=1}^{N}\frac{\mathbf{P}_j^2}{2M}+\sum_{i>j}U_0(\mathbf{R}_{ij})+\sum_i H_0(\mathbf{p}_i,\dot{\mathbf{p}}_i) - \sum_{i>j}\mathbf{p}_i\cdot\mathscr{T}_{ij}\cdot\mathbf{p}_j. \tag{2.2}$$

Here $\{\mathbf{R}_i,\mathbf{P}_i\}$ are the positions and linear momenta of the atoms, $\mathbf{R}_{ij}=\mathbf{R}_i-\mathbf{R}_j$ is the vector connecting atoms i and j, $\{\mathbf{p}_i,\dot{\mathbf{p}}_i\}$ are the instantaneous dipoles and their associated velocities, $U_0(\mathbf{R}_{ij})$ is the short-range interaction potential between atom i and j arising from the overlap interactions between the atoms, and the dipole–dipole propagator is

$$T_{ij}^{\mu\nu}=\frac{3R_{ij}^{\mu}R_{ij}^{\nu}-\delta^{\mu\nu}R_{ij}^2}{R^5}. \tag{2.3}$$

In this paper, tensors are represented by caligraphic symbols, upper indices $\mu\nu$ stand for coordinate components and the lower indices i and j stand for particles.

The large separation between the time scales of the dispersion oscillator motion and the "nuclear" motion permits us to treat the nuclear motion adiabatically. In this Born–Oppenheimer approximation, we can omit the nuclear kinetic energy term, $P_j^2/2M$, from Eq. (2.2). We can study the dynamics of the instantaneous dipoles for each liquid configuration and average over all possible arrangements. In other words, the nuclear degrees of freedom need not be treated as dynamical variables. In this approximation the Hamiltonian is

$$H_{\mathrm{BO}}=\sum_{i>j}U_0(R_{ij})+H_{\mathrm{DO}}, \tag{2.4}$$

where the Drude oscillator Hamiltonian is

$$H_{\mathrm{DO}}=\sum_i H_0(\mathbf{p}_i,\dot{\mathbf{p}}_i)-\sum_{i>j}\mathbf{p}_i\mathscr{T}_{ij}\mathbf{p}_j. \tag{2.5}$$

The imaginary time path integral representation of the quantum partition function of the Drude oscillator system is[16]

$$Z(\{R_i\})=\exp\left[-\beta\sum_{i>j}U_0(R_{ij})\right]\int[\mathscr{D}\mathbf{p}](u) \times\exp\left\{-\beta\int_0^1 du\left[\sum_i\frac{1}{2\alpha b^2}\left(\frac{\partial\mathbf{p}_i(u)}{\partial u}\right)^2 + \sum_i\frac{\mathbf{p}_i^2(u)}{2\alpha^2}-\sum_{i>j}\mathbf{p}_i(u)\cdot\mathscr{T}_{ij}\cdot\mathbf{p}_j(u)\right]\right\}, \tag{2.6}$$

where $b=\beta\hbar\omega$ is the ratio of the phonon energy of the Drude oscillator to the average thermal energy. For $b\gg1$ quantum effects are important.

Transformation to the normal-mode coordinates $\tilde{p}_i$ defined by

$$p_i(u)=\sum_{n=-\infty}^{n=\infty}\tilde{p}_{in}e^{-i2\pi nu} \tag{2.7}$$

diagonalizes the kinetic and quadratic potential terms allowing immediate integration of each mode independently. The quantum partition function thus takes the form of a product of classical partition functions for the individual modes

$$Z_{\mathrm{DO}}(\{R_i\})=\left[\prod_{n=-\infty}^{+\infty}Z_{\mathrm{cl}}^{(n)}(\{R_i\})\right]\exp\left[-\beta\sum_{i>j}U_0(R_{ij})\right], \tag{2.8}$$

where the partition function for a particular mode is

$$Z_{\mathrm{cl}}^{(n)}(\{R_i\})=\left[\left(\frac{2\pi\alpha_n}{\beta}\right)^N\frac{1}{\det\mathscr{A}_n}\right]^{1/2} \tag{2.9}$$

in which α_n, given by

$$\frac{1}{\alpha_n}=\frac{1}{\alpha}\left[\left(\frac{2\pi n}{b}\right)^2+1\right], \tag{2.10}$$

is the generalization of the classical static polarizability α and $\mathscr{A}_n$ is defined as

$$\mathscr{A}_n=\mathscr{I}-\alpha_n\mathscr{T}, \tag{2.11}$$

where $\mathscr{T}$ is the matrix defined in Eq. (2.3). Obviously, α_0 is the classical polarizability α.

The potential of mean force of the nuclear coordinates after averaging over the quantum paths for the Drude oscillators is

$$W(\{R_i\})=\sum_{i>j}U_0(R_{ij})+\frac{1}{2}kT\sum_{n=-\infty}^{+\infty}\ln(\det\mathscr{A}_n), \tag{2.12}$$

where the last term gives the quantum many-body dispersion energy of the system which adds to the two-body repulsive energy given by the first term. In simulations only the two-body part of the dispersion interaction is usually included by incorporating it into a simple pairwise potential. On the other hand, the above expression contains many-body effects to all orders in the dipole–dipole interaction.

Dipolar interactions between dispersion oscillators shift the ground state energy. This shift gives the dispersion energy of the system and can be computed from the quan-

tum partition function. The dispersion interaction is then given by the last term in Eq. (2.12),

$$U_{\mathrm{DISP}}(\{R_i\}) = +\frac{1}{2} kT \sum_{n=-\infty}^{+\infty} \ln(\det \mathscr{A}_n). \tag{2.13}$$

Introducing the operator identity,

$$\ln[\det \mathscr{A}] = \mathrm{Tr} \ln \mathscr{A}$$

and using the Taylor expansion of $\ln \mathscr{A} = \ln[\mathscr{I} - \alpha\mathscr{T}]$ we rewrite Eq. (2.13) as

$$U_{\mathrm{DISP}}(\{R_i\}) = -kT \sum_{n=-\infty}^{+\infty} \sum_{m=1}^{+\infty} \frac{1}{2m} \mathrm{Tr}(\alpha_n \mathscr{T})^m. \tag{2.14}$$

The summation over the modes, n, can be carried out using the identity

$$\sum_{n=-\infty}^{+\infty} \frac{1}{[1+(2\pi n/b)^2]^2} = \frac{1}{2}\left\{\frac{(b/2)}{\coth(b/2)} - \frac{(b/2)^2}{[\sinh(b/2)]^2}\right\}. \tag{2.15}$$

For atomic or molecular systems studied here, the factor b is very large, normally of order 10^3. The limit of the summation Eq. (2.15) for large b is $b/4$. Consequently, the leading two-body interaction term can be reduced to

$$U_{\mathrm{DISP}}(\{R_i\}) = -kT \sum_{ij} \frac{b}{16} \alpha^2 \mathrm{Tr}\, \mathscr{T}_{i,j}^2$$

$$= -\sum_{i>j} \frac{3}{4} \hbar\omega\alpha^2 \frac{1}{r_{ij}^6}. \tag{2.16}$$

This is exactly the asymptotic ground state energy shift that can be derived from second-order quantum perturbation theory. In the $(b \to \infty)$ limit when quantum effects dominate, the N-body Drude system remains in its ground state for every nuclear configuration. In this limit the electrons move so fast that they are always in the ground state at every instant of nuclear motion.

Equation (2.16) can be easily generalized to interaction potentials between different kinds of atoms. In this case, we have

$$U_{\mathrm{DISP}}(\{R_i\}) = -\sum_{i>j} \frac{3}{4} \hbar\alpha_i\alpha_j\omega_{ij} \frac{1}{r_{ij}^6}, \tag{2.17}$$

where $\omega_{ij} = 2\omega_i\omega_j/(\omega_i+\omega_j)$ and subscripts i and j denote the parameters of the specified particles. If $\omega_i = \omega_j$ and $\alpha_i \neq \alpha_j$,

$$U_{\mathrm{DISP}}(\{R_i\}) = -\sum_{i>j} c_i c_j \frac{1}{r_{ij}^6} \tag{2.18}$$

which is the same form as proposed by Dykstra.[14]

The next order in the expansion series of Eq. (2.14) gives the three-body quantum correction. In principle, we can carry on the procedure and obtain all the many-body interaction terms. The high performance of the modern computer makes it possible to diagonize the matrix $\mathscr{A}$ exactly for a reasonably large system that resembles a fluid and thus makes it possible to simulate polarizable fluids including both many-body dispersion forces and many-body electrical induction. However, in most calculations, the ground state energy shift is incorporated in the pair potential of the nuclear degree of freedom, such as a hard sphere or Lennard-Jones potential.

The summation over the normal modes in Eq. (2.14) can be simplified using

$$\sum_{n=-\infty}^{\infty} \frac{1}{m}\left(\frac{1}{1+(2\pi n/b)^2}\right)^m \equiv bC_m(b), \tag{2.19}$$

where

$$\lim_{b\to\infty} C_m(b) = \frac{(2m-3)!!}{(2m)!!}. \tag{2.20}$$

Therefore, the ground state energy shift can be expressed as

$$V = -\frac{\hbar\omega}{2} \sum_{m=2}^{\infty} \alpha^m C_m(b) \mathrm{Tr}\, \mathscr{T}^m. \tag{2.21}$$

The $m=1$ term vanishes because $\mathscr{T}$ is traceless, the second term yields the two-body London dispersion potential, and the third term yields the three-body Axilrod–Teller potential. The above equations give the many-body dispersion potential in terms of $\mathscr{T}$ and serve as the basis of our numerical calculations.

For finite systems such as clusters, the matrix $\mathscr{T}$ can be diagonalized, yielding eigenfrequencies and normal modes of the Hamiltonian. The ground state energy shift is then given by the shift of the frequencies

$$V = \sum_{i=1}^{3N} \frac{\hbar\omega}{2} (\sqrt{1-\alpha\lambda_i} - 1), \tag{2.22}$$

where $\{\lambda_i\}$ are the eigenvalues of $\mathscr{T}$. By expanding the perturbed frequencies in powers of α and recognizing that the trace is invariant under rotations of the whole system we are able to recover Eq. (2.21). The two expressions are identical for clusters.

Equation (2.21) explicitly gives the contributions from two-body forces, three-body forces, etc., and converges very rapidly. This treatment is general and can be applied to other problems such as the one presented in the next section of this paper where the usage of Eq. (2.22) is limited by numerical accuracy (because the interaction energy is then a small difference between two large quantities).

It is a simple matter to determine the electrical response of clusters in a static external field. For a single Drude oscillator the response coefficient is the polarizability α. In a cluster of N Drude oscillators, the total induced dipole will again be proportional to the external field and the response coefficient will be the polarizability tensor of the cluster. If one ignores the interaction between the induced dipoles the polarizability tensor of the cluster will be spherical with magnitude $N\alpha$, but when dipole–dipole interactions are included, the polarizability tensor is determined by the inverse of the matrix $\mathscr{A}$ defined in Eq. (2.11). The components of the polarizability tensor of the cluster divided by $N\alpha$, denoted by $\kappa^{\mu\nu}$, are

$$\kappa^{\mu\nu}=\frac{1}{N}\sum_{ij}(\mathscr{A}_0^{-1})_{ij}^{\mu\nu}, \tag{2.23}$$

and the total induced dipole of a cluster due to an external field is

$$\sum_{i=1}^{N} p_i^{\mu}=N\alpha\kappa^{\mu\nu}\mathbf{E}_{\nu}. \tag{2.24}$$

Clearly, $\kappa^{\mu\nu}$ will be a unit tensor if we ignore many-body interactions in the cluster.

In the next section we apply the matrix expansion approach to predict the leading term of the interaction energy between two clusters. This matrix approach is applied to clusters and fluids in the final section.

III. THE INTERACTION BETWEEN TWO CLUSTERS

Consider two clusters composed, respectively, of N_1 and N_2 interacting Drude oscillators. Each cluster responds to an external field as a whole, not as N independently fluctuating dipoles. If two such clusters are separated by a large distance R, the leading long-range term in the potential is proportional to R^{-6} and the proportionality constant will reflect the full many-body polarization of each cluster. The long-range potential can thus be written as

$$V_{N_1,N_2}(R)=-\frac{3}{4}N_1N_2\hbar\omega\alpha^2F\frac{1}{R^6}, \tag{3.1}$$

where F represents the deviation of the interaction from the value obtained from the summation of the independent site interactions between the atoms on one cluster and the atoms on the other. If the many-body effects are unimportant then $F=1$, and its deviation from unity gives a measure of the importance of these effects.

Since the distances between molecules inside the clusters are much smaller than those between the clusters, the intermolecular interaction between clusters can be regarded as a small perturbation of the energy and the distances between all intercluster pairs can be approximated by the distance between cluster centers of mass. Thus $V'=-\Sigma_{i\in1,j\in2}\mathbf{p}_{i1}\cdot T_{12}\cdot\mathbf{p}_{j2}$, where the index i is summed over all atoms on cluster 1, j is summed over all atoms on cluster 2 and T_{12} is the dipole propagator between the centers of mass of clusters 1 and 2. Therefore, the ground state energy shift can be expressed as

$$e^{-\beta\Delta E}=\langle e^{-\int_0^1 V'(u)du}\rangle, \tag{3.2}$$

where the average is taken over the path summations of the two noninteracting clusters. We show in the Appendix that the asymptotic potential now takes the form of Eq. (3.1) with

$$F=\frac{1}{6N_1N_2}\sum_{\lambda_1\lambda_2}[4(\Gamma_{\lambda_1}^{11}\Gamma_{\lambda_2}^{11}-\Gamma_{\lambda_1}^{12}\Gamma_{\lambda_2}^{21}-\Gamma_{\lambda_1}^{13}\Gamma_{\lambda_2}^{31})+(\Gamma_{\lambda_1}^{22}\Gamma_{\lambda_2}^{22}+\Gamma_{\lambda_1}^{33}\Gamma_{\lambda_2}^{33}+\Gamma_{\lambda_1}^{23}\Gamma_{\lambda_2}^{32})]f_{\lambda_1\lambda_2}, \tag{3.3}$$

where the quantities Γ_{λ}^{ij} and $f_{\lambda_1\lambda_2}$ are defined in the Appendix. It can be easily verified that Eq. (3.3) yields $F=1$ when many-body polarization is ignored. $F-1$, which is the measure of the importance of many-body effects, will be an increasing function of the polarizability α.

IV. NUMERICAL RESULTS

A. Clusters

The structure of van der Waals clusters has been the subject of numerous important theoretical studies. Most of these studies are based on a pairwise additive L-J potential.[3] It was found that three symmetry patterns based on pentagonal, tetrahedral, and icosahedral growth, give particularly stable structures and low energies. It is known that many-body forces give significant contributions to the surface tension of liquids and thus it is of interest to determine if they might play an important role in determining the structures of small clusters where surface energies should be relatively more important than in liquids.

The many-body polarization contributions to the potential energy of compact clusters should be repulsive. This is because the leading many-body term, the three-body Axilrod–Teller potential,[17] is positive on the average and the expansion series, Eq. (2.21) for $m\geqslant4$ has alternating signs and converges to small values. Thus it is to be expected that the many-body contribution to the potential will reduce the attractions between the clusters, thereby giving rise to smaller binding energies. The changes in cluster energetics induced by many-body forces will be manifested in several ways: the total potential energy including the full many-body contribution will be higher than the total L-J potential for the same nuclear configuration, the minimum energy configurations will be less compact than for the L-J potential, and the clusters will be softer, i.e., they will have smaller force constants and lower vibrational frequencies.

In the following we adopt a simple model for the potential parameters. The Lennard-Jones dispersion parameter is $C_6=4\epsilon\sigma^6$. This model overestimates the contribution from the lowest-order two-body dipole–dipole approximation because it attempts to include the effect of the higher dispersion forces arising from the dipole–quadrupole, quadrupole–quadrupole, etc., interactions, terms that make the potential more negative than the dipole–dipole term as the internuclear distance becomes smaller. Since for the Drude oscillator $C_6=\frac{3}{4}\alpha^2\hbar\omega$ [see Eq. (2.16)], we fit the Drude oscillator parameters so that

$$4\epsilon\sigma^6=\tfrac{3}{4}\alpha^2\hbar\omega \tag{4.1}$$

or

$$\hbar\omega=\frac{16\epsilon}{3\alpha^{*2}}, \tag{4.2}$$

where $\alpha^*=\alpha/\sigma^3$ is the reduced polarizability. For this choice of parameters $\{\alpha^*,\omega\}$ the Drude oscillator model Eq. (2.21) will reduce to the L-J 12–6 potential when the many-body and higher-order effects are ignored. A good example of this is xenon $\{\epsilon=229\text{ K}, \sigma=4.055, \alpha^*=0.06\}$ where it is found that $\omega=1.035$ in atomic units. It is important to recognize that this choice may overestimate the

TABLE I. Total energy and many-body contributions of minimum energy configurations according to the pentagonal growth sequence.

n	E_t(Total)	E_m(Many-body)	E_3(Three-body)	E_m/E_t	E_3/E_t
7	−15.418 63	1.086 710	1.434 358	7.048 032	9.302 759
8	−18.512 45	1.308 970	1.750 403	7.070 755	9.455 275
9	−22.428 48	1.684 784	2.268 168	7.511 806	10.112 89
10	−26.351 10	2.071 318	2.806 570	7.860 460	10.650 67
11	−30.298 52	2.467 333	3.356 192	8.143 410	11.077 08
12	−34.917 39	3.050 014	4.156 696	8.734 943	11.904 37
13	−40.477 84	3.848 748	5.252 208	9.508 284	12.975 51
14	−43.782 37	4.062 518	5.581 526	9.278 890	12.748 34
15	−47.895 18	4.427 030	6.110 723	9.243 164	12.758 54
16	−52.016 31	4.798 719	6.653 800	9.225 411	12.791 76
17	−56.115 87	5.190 215	7.221 983	9.249 104	12.869 77
18	−60.761 53	5.768 747	8.038 955	9.494 078	13.230 34
19	−66.117 31	6.541 793	9.097 469	9.894 220	13.759 59
20	−70.283 04	6.893 072	9.630 052	9.807 590	13.701 82
21	−74.402 44	7.281 527	10.210 01	9.786 678	13.722 68
22	−78.481 78	7.666 101	10.785 44	9.768 001	13.742 60
23	−82.522 07	8.035 690	11.338 84	9.737 625	13.740 37
24	−86.564 02	8.433 032	11.929 89	9.741 961	13.781 58
25	−91.304 86	8.954 021	12.682 16	9.806 731	13.889 91
26	−96.135 96	9.439 398	13.384 73	9.818 800	13.922 71

many-body dipole–dipole interaction and better choices are possible as we will show in another publication.[18]

To illustrate these effects quantitatively, we have performed calculations for clusters of $N=7$ to 26 atoms whose configurations are generated according to the pentagonal growth sequence outlined by Hoare and Pal.[3] Initial configurations based on the pentagonal geometry are generated from approximate minimum energy coordinates. The Monte Carlo method is then employed to search for the minimum energy configuration of the system with L-J forces. The minimum energies thus obtained agree well with those provided by Hoare and Pal in their review paper.[3] The polarization energies were calculated with both Eqs. (2.21) and (2.22) and with the static polarizability $\alpha^*=0.06$. The series expansion method converges very rapidly and terms with $m>10$ in Eq. (2.21) are negligible so that the two methods agree with each other to within the limits of computer precision. In Table I, we list various contributions to the total energies of the clusters: E_t the energy of the full potential, E_3 the contribution of the three-body Axilrod–Teller potential, E_m the contribution of all the many-body terms, the percentage ratio of E_m to E_t, and the percentage ratio of E_3 to E_t. In Fig. 1 we plot these data vs n, the number of particles in the clusters. Obviously, the three-body contribution is about 13% of the total energy, but when all the many-body terms are included the total many-body contribution falls to approximately 10% of the total energy. These curves show sharp changes at cluster sizes of $N=7$, 13, and 19 where the structures shrink a bit because of icosahedral shell closure. These sharp features are much more pronounced when many-body polarization energy is included. This indicates that the many-body polarization energy is more sensitive to the nuclear configuration than the Lennard-Jones energy. We also calculate the many-body polarization energy as a function of polarizability. In Fig. 2 these results for clusters

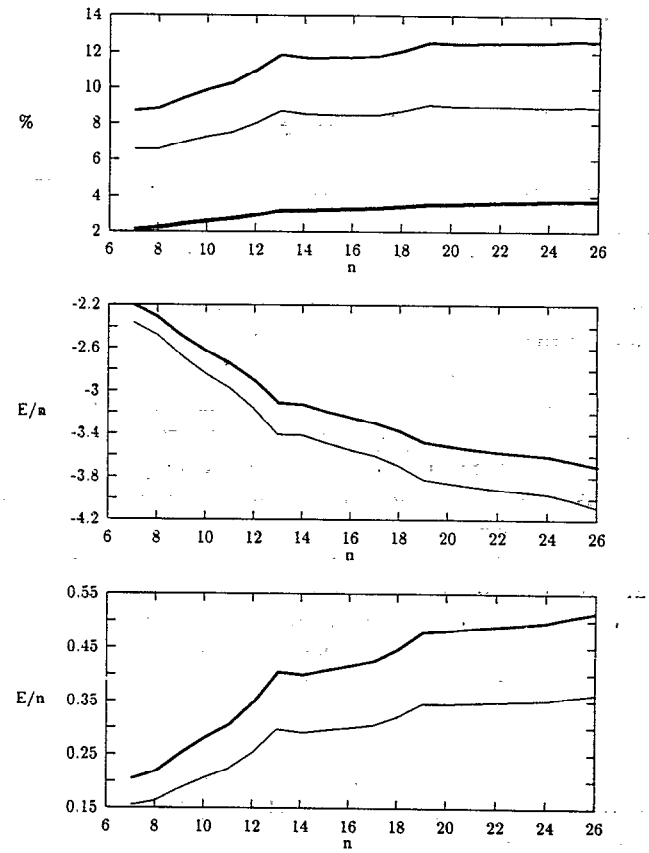

FIG. 1. Data listed in Table I plotted as a function of the number of particles. The top panel gives the polarization energy as a percentage of the total energy (which includes the two-body short range interaction) where the upper curve is for three-body correction, the middle curve is for many-body correction, the low one is for the contribution from terms other than the three body. In the next panel, the solid curve is the total energy (including many-body correction) per particle, and the bold curve is the L-J potential per particle. In the last panel, the solid curve is the three-body polarization energy per particle, and the bold curve is the many-body polarization energy per particle.

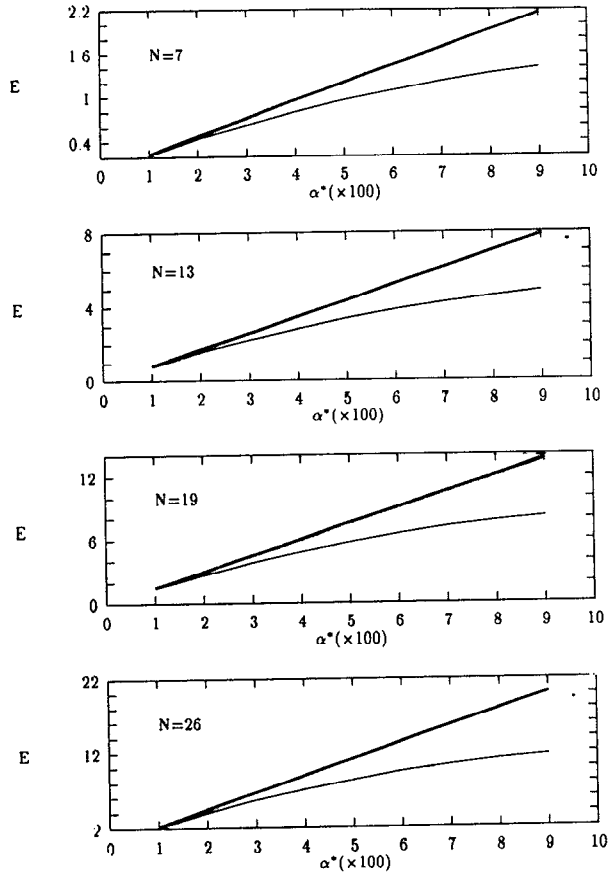

FIG. 2. The many-body corrections (the solid curve) and the three-body corrections (the bold curve) plotted as a function of the polarizability α. The four panels from the top to the bottom correspond to the clusters 7, 13, 19, 26, respectively.

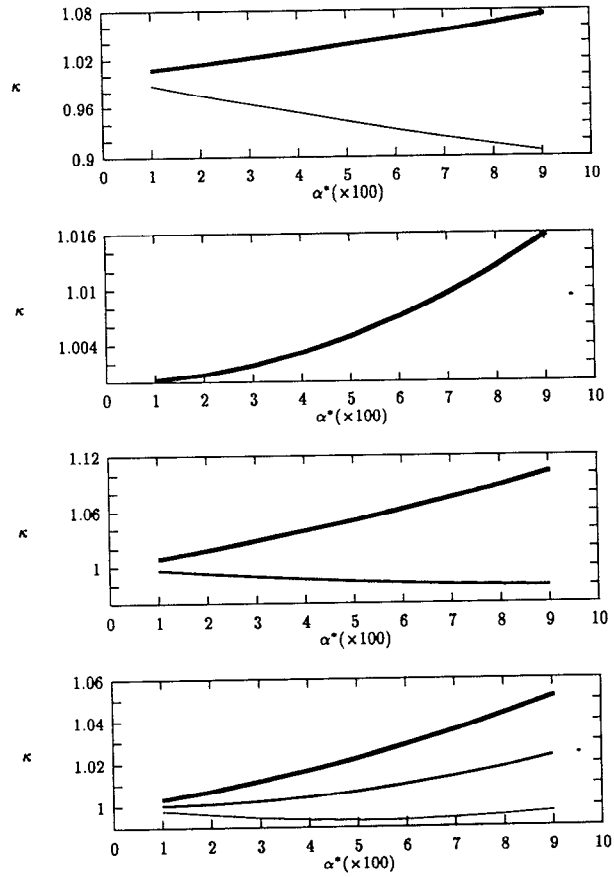

FIG. 3. The three principal values of the normalized polarizability tensor κ defined in Eq. (2.23) are plotted as functions of the single atom polarizability α. The four panels from the top to the bottom correspond to the clusters 7, 13, 19, 26, respectively. In the first panel the upper curve corresponds to two degenerate principle values (bold curve) and the lower curve corresponds to one nondegenerate principle value; and in the second panel the bold curve is three-fold degenerate; in the third panel the lower curve is doubly degenerate and the upper curve (bold curve) is singly degenerate; in the fourth panel all the principle values are different (nondegenerate).

$N=7$, 13, 19, and 26 are plotted along with the three-body corrections. The three-body correction is linear in α, while the higher order corrections grow nonlinearly with α.

We now address the question of how the polarizability of clusters varies with cluster size and geometry. Since the cluster is generally not isotropic we perform a rotational transformation to diagonalize the tensor κ defined in Eq. (2.23). In Fig. 3, we plot the three principle values of the tensor κ as functions of the "atomic" polarizability α for cluster $N=7$, 13, 19, and 26. The configurations of these clusters are the same as the minimum energy structures discussed in the preceding paragraph. The more anisotropic the cluster the larger will be the differences between the principle values of the polarizability. Thus we see that because the cluster $N=13$ is a closed shell icosahedron the principle polarizabilities are equal whereas for the open clusters $N=7$, 19, and 26 the principle moments are more degenerate. The $N=7$ and 19 clusters are symmetric tops and thus have two distinct principle values whereas the $N=26$ cluster is fully anisotropic.

Next we try to locate the minimum energy configuration under the full potential. Because the CPU time required for the calculation of the polarization energy is large, we have simplified the calculation by scaling the coordinates of the whole cluster while fixing the geometry. The minimum energy geometry thus found, although not exact is very close to the real minimum. In Fig. 4 we plot the total L-J energy and the energy including many-body polarization vs the scaling parameter s. The energy zero corresponds to the minimum energy configuration for the clusters interacting through the two-body L-J potential ($s=1$). We list the scaling parameters and energies corresponding to the minimum potential energy for clusters $N=7$, 13, 19, and 26 in Table II. The energy reaches a minimum at about $s=1.01$ which implies the volumes of the clusters expand $\approx 3\%$ after the many-body polarization energy is taken into account. Finally, in Table II we list the force constant $K=\partial^2 V/\partial s^2$, which correspond to the symmetric stretch frequencies of these cluster at their potential minima. It can be seen that the force constant softens by $\approx 10\%$ when many-body polarizations are included. We have also found the true minimum energy configuration for the $N=7$ cluster. In a pentagonal bipyramid, there are only two parameters to scale, the side of the pentagon and the distance between the axial particles. The

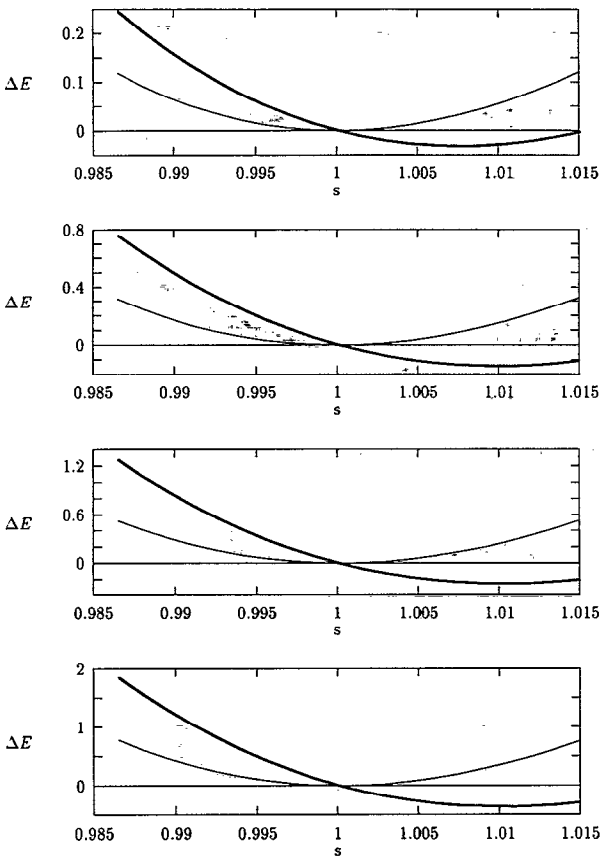

FIG. 4. The L-J energy (the solid curve) and the total energy including many-body corrections (the bold curve) versus the scaling parameter s. The energy zero is taken to be the minimum energy for the $s=1$ configuration, which is the minimum configuration for the two-body L-J potential. The four panels from the top to the bottom correspond to the clusters 7, 13, 19, 26, respectively.

scaling parameters thus found are 1.006 for the side and 1.0135 for the axial distance and the minimum energy is -15.453 compared to -16.505 for the L-J potential. Although there is a distortion of the geometry due to the many-body effects, the effect is minor and the preceding conclusions based on one-parameter scaling calculations are expected to be valid.

The minimum energy configurations generated by a tetrahedral growth process are also changed little from the two-body structures. More significantly, the observation that the pentagonal structure is more stable than other structures for small clusters[3] remains valid when many-body forces are included.

TABLE II. The minimum energy ΔE inluding the many-body correction,the scaling parameter s, and the force constant K.

n	s(min)	ΔE	K(total)	K(L-J)
7	1.0075	−0.032	0.0024	0.0027
13	1.01	−0.145	0.0063	0.0072
19	1.0105	−0.225	0.0103	0.0118
26	1.0105	−0.368	0.0154	0.0174

B. Liquids

The effect of many-body polarization on polarizable liquid xenon was also studied. For this liquid, we use a reduced density $\rho^*=\rho\sigma^3=0.38$, and a reduced temperature $T^*=0.612$, where the L-J parameters are $\sigma=4.05$ A and $\epsilon=299$ K and the reduced polarizability $\alpha^*=0.06$. A 108-particle system with periodic boundary conditions was simulated. Configurations are generated according to the L-J potential using a Metropolis Monte Carlo method with the step size adjusted to yield about 50% acceptance rate. The effects of periodic boundary conditions on the dipoles were included using Ewald summation techniques.[19] The extra potential due to the many-body polarization was included as a weighting function for each nuclear configuration (umbrella sampling). The average of an arbitrary property A is then given by

$$\langle A\rangle_{\text{many-body}}=\frac{\langle A\exp[-\beta(V_{\text{many-body}}-V_{\text{LJ}})]\rangle_{\text{LJ}}}{\langle\exp[-\beta(V_{\text{many-body}}-V_{\text{LJ}})]\rangle_{\text{LJ}}}, \tag{4.3}$$

where the subscripts on $\langle\rangle$ indicate the potential used in the Monte Carlo sampling. This is the standard umbrella sampling technique. After equilibrium was reached, the many-body correction was calculated after every 100 passes and data was accumulated over 1000 noncorrelated configurations. In Fig. 5 the pair correlation function is given for the two-body L-J and many-body simulations. We observe a decrease of the peak heights and a shifting out of the peak positions. These changes are attributable to the repulsive nature of the many-body polarization force.

In Fig. 5 we also plot the absorption spectrum of the interacting Drude oscillators for both the liquid whose structure is determined only by the two-body L-J forces and for the liquid whose structure is determined by the full many-body force. For the definition of the absorption spectrum and related matters we refer the reader to a forthcoming paper.[7] We observe that the spectrum of the liquid with many-body polarization effects included has a narrower bandwidth and a higher peak. This is consistent with the conclusion that the many-body correction is repulsive and tends to loosen the structure by as much as 10% in xenon.

C. Attractive interaction of two clusters

Following the above formulation, we are able to calculate the long-range attraction potential between two polarizable clusters. The two clusters are the minimum configurations of the $N=7$ cluster corresponding to the L-J potential. The correction coefficient F calculated from Eq. (3.3) is 1.05 for $\alpha=0.06$ and 1.1 for $\alpha=0.1$. This increased interaction results from the fact that the polarizability of each cluster is larger because of internal dipole–dipole interactions and because the clusters perturb the dipole distributions of each other.

Equation (2.22) can not be used to calculate the long-range interaction between two clusters because this energy is very small compared to the intercluster polarization energy, thus leading to problems with numerical precision.

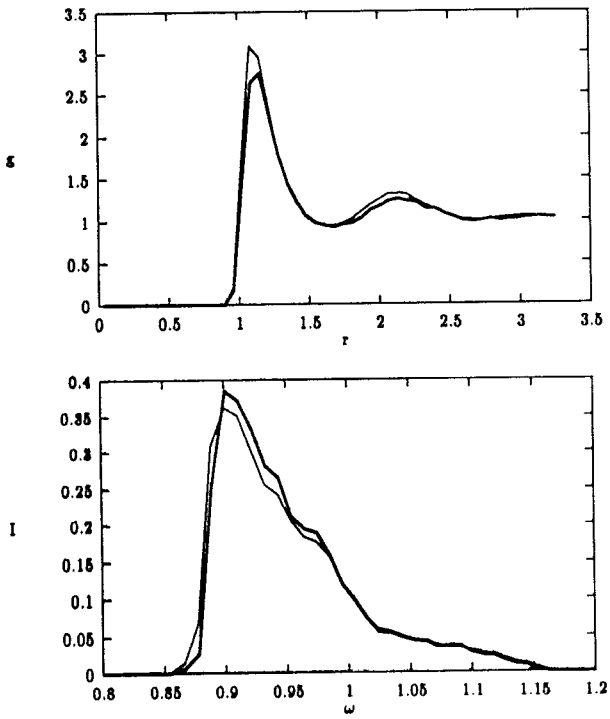

FIG. 5. The pair correlation functions (the upper panel) and the absorption spectra (the lower panel) for the polarizable liquid Xe described in the text. The solid curve is for the L-J potential; and the bold curve is for the full potential including the many-body polarization correction.

Because of this, the perturbation expansion Eq. (2.21) turns out to be the only alternative.

V. SUMMARY

In this paper computer simulations on polarizable clusters and homogeneous fluids composed of harmonious atoms interacting through dipole–dipole forces have shown that

(1) The minimum energy structures of such small clusters have essentially the same geometries as the Hoare and Pal structures of two-body L-J clusters. Small distortions from the Hoare and Pal structures are observed. A more detailed conformation search will be required to confirm this invariance of the geometries but this will be done in conjunction with our soon to be reported work on the full Coulomb interaction between the dispersion oscillators.

(2) The clusters expand by $\approx 3\%$ compared to the Hoare and Pal clusters for the polarizability typical of Xe.

(3) The vibrational frequencies of the clusters are smaller than for the Hoare and Pal clusters. We determined that for Xe clusters the breathing-mode frequency is reduced by $\approx 10\%$

(4) Many-body forces have a small effect on the structure of liquids; nevertheless, they give a measurable reduction in the first peak of the radial distribution function of liquid Xe.

(5) The many-body polarization interaction increases the polarizability of clusters and liquids.

(6) Many-body polarization gives rise to a measurable increase in the long-range interaction between van der Waals clusters. For Xe_7 clusters the long-range interaction is increased by 5% over the site–site L-J interaction.

ACKNOWLEDGMENTS

We gratefully acknowledge financial support of this work by the National Science Foundation (Grant No. CHE-87-00522) and the National Institutes of Health (Grant No. 1 RO1 GM43340-01A1). We thank Dr. Rama Krishna and Mr. Michael New for useful discussions about this work.

APPENDIX: A LONG RANGE CLUSTER–CLUSTER INTERACTION ENERGY

Writing the potential in Eq. (3.2) in terms of normal modes and taking a cummulant expansion to second order gives

$$-\beta\Delta E=\frac{1}{2}\sum_{n=-\infty}^{\infty}\mathrm{Tr}[\Gamma_1(n)T\Gamma_2(n)T] \tag{A1}$$

in which $\Gamma_I(n)$ is defined as

$$\Gamma_I^{\mu\nu}(n)=\beta\sum_{i,j\in I}\langle\tilde{p}_{in}^{\mu}\tilde{p}_{jn}^{\nu}\rangle=\alpha_n\sum_{i,j}(\mathscr{A}_n^{-1})_{ij}^{\mu\nu}, \tag{A2}$$

where α_n and $\mathscr{A}_n$ are defined by Eqs. (2.10) and (2.11) and $I=1, 2$ is an index specifying the cluster. When $\beta\hbar\omega$ is large, the convergence of Eq. (A1) with the number of normal modes is very slow. Fortunately, we can complete the summation of the normal modes analytically.

Since it is possible to determine the eigenvalues λ of $\mathscr{T}$ for each cluster, we recast $\Gamma(n)$ as

$$\Gamma(n)=\sum_{\lambda}\Gamma_\lambda\frac{\alpha_n}{1-\alpha_n\lambda}, \tag{A3}$$

where $\Gamma_\lambda^{\mu\nu}=\Sigma_i S_{i\lambda}^{\mu}\Sigma_j S_{j\lambda}^{\nu}$ and where S is the transformation matrix that diagonalizes $\mathscr{T}$ and $\{\lambda_i\}$ is the set of eigenvalues of this matrix. Hence, the ground state energy shift becomes

$$\frac{1}{2}\sum_{\lambda_1\lambda_2}\mathrm{Tr}(\Gamma_{\lambda_1}T\Gamma_{\lambda_2}T)\sum_{n=-\infty}^{\infty}\frac{\alpha_n}{1-\alpha_n\lambda_1}\frac{\alpha_n}{1-\alpha_n\lambda_2}. \tag{A4}$$

We shall perform the summation of normal modes first. In the large b limit the summation reduces to

$$\lim_{b\to\infty}\sum_{n=-\infty}^{\infty}\frac{\alpha_n}{1-\alpha_n\lambda_1}\frac{\alpha_n}{1-\alpha_n\lambda_2}=\frac{b}{4}\alpha^2 f_{\lambda_1\lambda_2}, \tag{A5}$$

where the function $f_{\lambda_1\lambda_2}$ is given by

$$f_{\lambda_1\lambda_2}=\frac{2}{(\eta_1+\eta_2)\eta_1\eta_2} \tag{A6}$$

in which η_i is related to the eigenvalue λ by $\eta_i=\sqrt{1-\alpha\lambda_i}$.

Substitution of Eqs. (A4)–(A6) into Eq. (A1) gives the interaction energy at low temperature between clusters,

$$\Delta E=-\frac{\hbar\omega}{8}\alpha^2\sum_{\lambda_1\lambda_2}\mathrm{Tr}(\Gamma_{\lambda_1}T\Gamma_{\lambda_2}T)f_{\lambda_1\lambda_2}. \tag{A7}$$

For the sake of convenience, we locate one cluster at the origin and the other at $\mathbf{R}=(R,0,0)$ so that the dipolar propagator is

$$\mathcal{T}=\begin{pmatrix}2&0&0\\0&-1&0\\0&0&-1\end{pmatrix}\frac{1}{R^3}. \tag{A8}$$

The asymptotic potential Eq. (A7) now takes the form of Eq. (3.1) with

$$F=\frac{1}{6N_1N_2}\sum_{\lambda_1\lambda_2}[4(\Gamma^{11}_{\lambda_1}\Gamma^{11}_{\lambda_2}-\Gamma^{12}_{\lambda_1}\Gamma^{21}_{\lambda_2}-\Gamma^{13}_{\lambda_1}\Gamma^{31}_{\lambda_2}) +(\Gamma^{22}_{\lambda_1}\Gamma^{22}_{\lambda_2}+\Gamma^{33}_{\lambda_1}\Gamma^{33}_{\lambda_2}+\Gamma^{23}_{\lambda_1}\Gamma^{32}_{\lambda_2})]f_{\lambda_1\lambda_2}. \tag{A9}$$

It can be easily verified that Eq. (A9) yields $F=1$ when many-body polarization is ignored. This is accomplished by setting the matrix S equal to the unit matrix and by letting λ_1 and λ_2 go to zero.

[1] J. A. Barker and M. L. Klein, Phys. Rev. B **7**, 4707 (1973).
[2] J. Miyazaki, J. A. Barker, and G. M. Pound, J. Chem. Phys. **64**, 3364 (1976).
[3] M. R. Hoare and P. Pal, Adv. Phys. **20**, 161 (1971).
[4] L. R. Pratt. Mol. Phys. **40**, 347 (1980).
[5] Z. Chen and R. Stratt, J. Chem. Phys. **95**, 2669 (1991).
[6] D. Chandler, K. S. Schweizer, and P. Wolynes, Phys. Rev. Lett. **49**, 1100 (1982).
[7] J. Cao and B. J. Berne (to be published).
[8] J. A. Barker, in *Rare Gas Solids*, edited by M. L. Klein and J. A. Venables (Academic, New York, 1984).
[9] C. E. Dykstra, J. Am. Chem. Soc. **94**, 6948 (1990).
[10] T. R. Horn, R. B. Gerber, J. J. Valentini, and M. A. Ratner, J. Chem. Phys. **94**, 6728 (1991).
[11] D. M. Leitner, J. D. Doll, and R. M. Whitnell, J. Chem. Phys. **94**, 6644 (1991).
[12] R. A. Aziz and M. Slaman, Mol. Phys. **58**, 679 (1986).
[13] J. J. Perez, J. H. Clarke, and A. Hinchliffe, Chem. Phys. Lett. **104**, 583 (1984).
[14] C. E. Dykstra, J. Am. Chem. Soc. **111**, 6168 (1989).
[15] H. Margenau and N. R. Kestner, *Theory of Intermolecular Forces* (Pergamon, Oxford, 1969).
[16] R. P. Feynman and A. R. Hibbs, *Quantum Mechanics and Path Integrals* (Wiley, New York, 1965).
[17] N. R. Kestner, Can. J. Chem. **55**, 1937 (1977).
[18] M. New, J. Cao, and B. J. Berne (to be published).
[19] S. W. de Leeuw, J. W. Perram, and E. R. Smith, Proc. R. Soc. London, Ser. A **373**, 27 (1980).